

In Vitro Investigation of Pacemaker Lead Heating Induced by Magnetic Resonance Imaging: Role of Implant Geometry

Giovanni Calcagnini, PhD,^{1*} Michele Triventi, EEng,¹ Federica Censi, PhD,¹ Eugenio Mattei, EEng,^{1,2} Pietro Bartolini, EEng,¹ Wolfgang Kainz, PhD,³ and Howard I. Bassen, EEng, MS³

Purpose: To evaluate the effect of the geometry of implantable pacemakers (PMs) on lead heating induced by magnetic resonance imaging (MRI).

Materials and Methods: In vitro experiments were conducted with two different setups, using fluoroptic probes to measure the temperature increase. The first experiment consisted of a rectangular box filled with a gelled saline and a pacemaker with its leads. This box was exposed in an MRI birdcage coil to a sinusoidal 64-MHz field with a calibrated whole-body specific absorption rate (WB-SAR) of 1 W/kg. The highest SAR and temperature increase (3000 W/kg, 12°C) occurred for the implant configuration having the largest area. The second experimental setup consisted of a human-shaped torso filled with gelled saline. In this setup the PM and its lead were exposed to a real MRI scanner, using clinical sequences with WB-SAR up to 2 W/kg.

Results: We found that higher heating occurs for configurations with longer exposed lead lengths and that right chest PMs showed the highest temperature and local SAR (11.9°C, 2345 W/kg), whereas the left chest PMs were less heated (6.3°C, 1362 W/kg). Implant geometry, exposed lead length, and lead area must be considered in the wide variation of temperature increases induced by MRI.

Conclusions: The amount of MRI-induced lead tip heating depends strongly on implant geometry, particularly the lead area, exposed lead length, and position of the implant in the phantom. Critical lead tip heating was found for the longer leads. Therefore, to minimize MRI-induced lead tip heating, the PM lead should be as short as possible.

Key Words: pacemaker; lead heating; fluoroptic measurements; implant geometry; radiofrequency
J. Magn. Reson. Imaging 2008;28:879–886.
 © 2008 Wiley-Liss, Inc.

MAGNETIC RESONANCE IMAGING (MRI) is now contraindicated for patients implanted with pacemakers (PMs) and implantable cardioverter-defibrillators (ICDs) (1–6). The potential effects of MRI on PMs, ICDs, and other active implantable medical devices (AIMDs) include: force and torque effects (7,8); an undefined reed-switch state within the static magnetic field (9); the potential risk of heart stimulation and inappropriate pacing (10,11); and heating effects at the lead tip (12–14).

The radio-frequency (RF) field used in MRI procedures may induce high current density around the lead tip (14–16). The amount of heating has been investigated by several groups who observed temperature increases from non-significant values up to tens of degrees. For example, Achenbach et al (12) reported a temperature increase of 63.1°C for a pacemaker lead; Rezaei et al (17) measured 25.3°C at the end of a deep brain stimulation electrode; Roguin et al (16) reported a maximum increase of 5.7°C at 3.54-W/kg average whole-body specific absorption rate (WB-SAR), as shown on MRI. Sommers et al (13), with a WB-SAR of 1.3 W/kg, obtained temperature increases ranging from 0.1° to 23.5°C, depending on the electrode type. Several factors influence the degree of heating:

1. The WB-SAR, which has been shown to correlate with temperature increase (18).
2. The cooling effect of the blood around the leads, which is seldom quantified.
3. The length and geometric structure of the lead.
4. The implant location, which may change the current induced.

Among these variables, we focused our attention on those characterizing real implants in clinical practice.

In this study we investigate the effect of the lead geometry and the lead and pacemaker can placement of

¹Department of Technology and Health, Italian National Institute of Health, Rome, Italy.

²Department of Information and System Science, University of Rome, "La Sapienza," Rome, Italy.

³Center for Devices and Radiological Health, United States Food and Drug Administration, Silver Spring, Maryland, USA.

Contract grant sponsor: Italian Ministry of Health.

*Address reprint requests to: G.C., Department of Technologies and Health, Istituto Superiore di Sanità, Viale Regina Elena 299, 00161 Roma, Italy. E-mail: giovanni.calcagnini@iss.it

Received September 11, 2006; Accepted July 8, 2008.

DOI 10.1002/jmri.21536

Published online in Wiley InterScience (www.interscience.wiley.com).

an implantable pacemaker on lead heating induced by MRI.

MATERIALS AND METHODS

We performed tests *in vitro* using two saline gel phantoms. The first test consisted of a rectangular box inside an MRI birdcage coil, and the second used a human-shaped phantom inside a real MRI system.

The first setup was used for heating measurements, using a dual-chamber pacemaker (Elect D; Sorin Biomedica CRM, Italy) and a biventricular three-chamber pacemaker (NewLiving CHF; Sorin Biomedica) and two different leads, one unipolar and the other bipolar (Models S80T and S80TB; Sorin Biomedica).

Based on the results obtained, we conducted a second series of experiments with a human-shaped phantom at an MRI clinical facility, using a dual-chamber pacemaker connected to a bipolar lead.

The lead had a length of 62 cm for all experiments, with an active tip area of 6 mm² and an active ring area of 36 mm². Both the rectangular box and the human-shaped phantom were filled with a gel composed of the following materials (in percent, by weight): 2% hydroxyethylcellulose (HEC; commercial name Natrosol); 97.64% water; and 0.36% sodium chloride. The gel has conductivity of 0.59 Sm⁻¹ at 64 MHz and heat capacity of 4178.3 J/kg K⁻¹ (19,20). These values have been chosen to most closely approximate those of human tissues at the frequencies of interest (i.e., 64 MHz), as specified by ASTM Standard F2182-02a (20).

A fluoroptic thermometer (Luxtron Model 3100; SMM Probes) was used to measure the temperature rise while minimizing perturbations to the RF fields (20). This thermometer has a resolution of 0.1°C and performs up to 8 measurements per second. A similar setup was used by Bassen et al (21) for an investigation of MRI-induced heating of metallic implants.

Rectangular Box Simulator

The rectangular box simulator consists of a rectangular box (60 × 30 × 20 cm) filled with saline gel. A 30 × 20-cm plastic grid submerged in the gel supports the implant and maintains consistent separation distances between the implant, phantom surface, and temperature probes. The grid can be adjusted so that the top of the implant can be positioned below the gel surface. The pacemaker and the leads were arranged in the gel 5 cm below the phantom's gel surface simulating the implanted lead in the human body. The phantom was placed in the middle of the MRI birdcage coil (i.e., with the center of mass of the box coinciding with the coil isocenter), housed in an anechoic chamber. The birdcage structure consists of 16 65-cm-long rods closed by two 62-cm-diameter external rings; the RF coil type is low-pass, with a tuning capacitor placed along each rod and a metallic shield. A 64-MHz quadrature sinusoidal excitation to the coil was delivered by a 100-W RF amplifier. The output power was measured continuously by a directional coupler and power meter. Using this setting, the RF energy delivered to the box corresponds to a WB-SAR of 1.0 W/kg (Fig. 1).

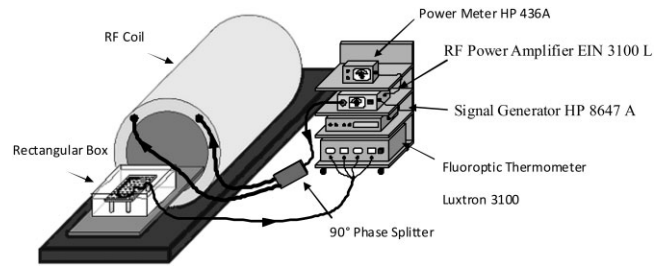


Figure 1. Schematic representation of the rectangular box simulator and the MRI simulator. The instruments used to feed the RF coil and measure the heating are also shown.

This value was obtained using a calorimetric method: the box, filled with 0.36% saline, was surrounded by a 2-cm-thick layer of foam rubber to ensure adiabatic conditions. Exposure to the RF signal lasted 1 hour and produced an average temperature increase of 0.9°C. Under these conditions, the WB-SAR can be determined according to the following SAR definition:

$$\text{WB SAR} = \frac{\Delta \text{Temp}}{\Delta \text{time}} \cdot C_p \quad [1]$$

where WB-SAR is specific absorption rate (W/kg), C_p is the specific heat of a lossy medium (joules/kg/°C), and $\frac{\Delta \text{temp}}{\Delta \text{time}}$ is the rate of temperature rise (°C/sec).

Human-Shaped Phantom

Experiments in a real MRI scanning system were performed using a human-shaped torso simulator (Fig. 2). The simulator is a transparent polyvinyl chloride (PVC) torso of a 70-kg male (Fig. 2A), with a 32-L internal volume (20). Inside the torso, a PVC grid supports the pacemaker, its leads, and the temperature probes (Fig. 2B). The torso was filled with the same saline gel as used in the simulated MRI experiments.

Implant Geometry Configuration

The actual geometry of a pacemaker implant may vary between patient2. The pacemaker can be implanted in the left or in the right side of the chest. Up to three leads may be advanced into the veins to reach the right atrium, the right ventricle, and the coronary vein. Because the length of the lead may not fit the patient's anatomy and size, the excess length is usually wrapped near or around the PM can.

In the experiments with the rectangular box, the total lead area of the implant was varied by wrapping the excess lead near the PM can or by changing the lead path. An example of varying the lead geometry is shown in Figure 3: When the lead forms loops around the PM the magnetic induction area is reduced (Fig. 3, upper panel); the lead area also changes by varying the lead path (Fig. 3, lower panel). For each configuration we computed the total lead area of the implant and the exposed lead length. The total lead area was calculated as the area delimited by the lead, the PM can, and the line connecting the lead tip to the PM center of mass

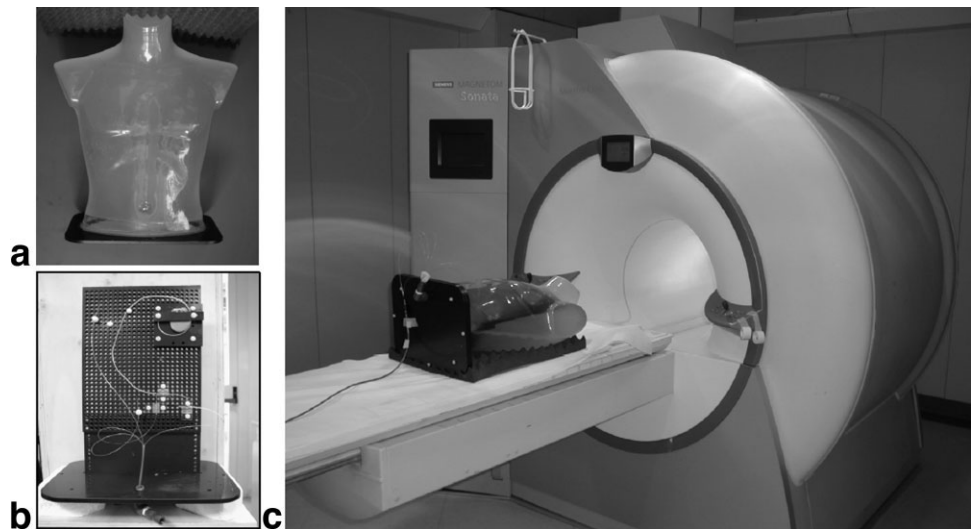


Figure 2. The torso simulator filled with gel (A) and equipped with a plastic grid, which supports the PM implant and the fluoroptic probes (B). The phantom prepared for a real MRI scan is shown in (C).

(Fig. 3, shaded areas); the exposed length was defined as the lead length not wrapped around the PM can. In the experiments using the rectangular box simulator the PM was always positioned as a left-side implant. In the human-shaped phantom, both right- and left-side implants were tested (Fig. 4).

Temperature Measurements and SAR Calculation

According to Bassen et al (21), local SAR is a reliable indicator of the maximum heating capability of an implant in vitro. In a previous study, Mattei et al (22)

investigated the positions and mounting of the temperature probes, which gives the minimum error for temperature and SAR measurements. The best positioning is obtained when the Luxtron probe tip (at the center of the pigmented part) is in direct contact with the lead tip or the ring electrode. In this configuration, the Luxtron probe tip and the lead tip or ring electrode are perpendicular to each other. Care was taken to ensure contact of the sensitive region of the Luxtron probe (center of the pigmented end of the Luxtron probe) and the lead tip or ring electrode. This configuration is also mechanically stable and reproducible. Another probe was used to monitor the temperature increase of the PM can. Last, a fourth probe measured the gel temperature 6.5

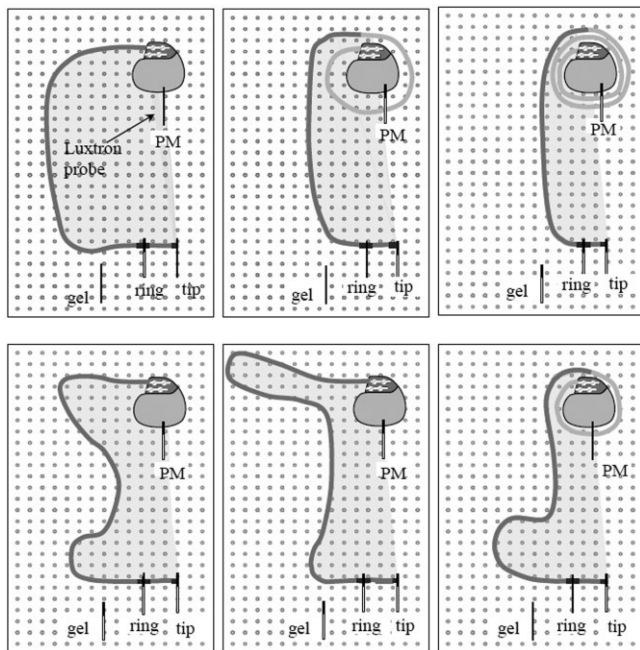


Figure 3. Examples of implant configurations tested in the MRI simulator. Lead area has been changed both by wrapping the lead around the PM (top panel: no-loop, 1-loop, and 2-loops) and/or by changing the lead path (bottom panel). The lead area of the implant (shaded) and the effective lead length (dark gray) are depicted. The positions of the optical probes are also shown (gel, ring electrode, lead tip, and PM case).

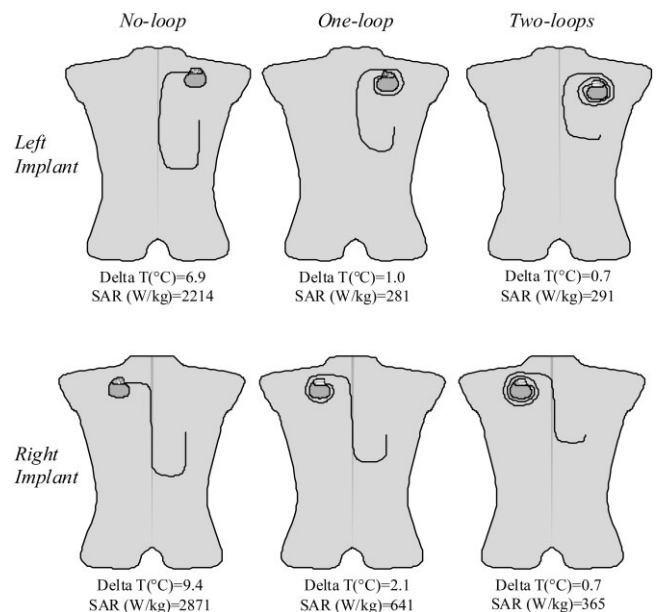


Figure 4. The six implant configurations tested in a real MRI using the human-shaped phantom: no-loop, 1-loop, and 2-loops for both left and right chest implantation. Local SAR and heating at the lead tip during a short fast spin-echo sequence, with WB-SAR of 1.94 W/kg (right implant) and 1.96 W/kg (left implant), are also shown.

Table 1
Main Parameters of MRI Clinical Sequences Used during Human-Shaped Phantom Experiments in a Real MRI Scanner

Siemens sequence name	Sequence type	TR (msec)	TE (msec)	Flip angle (°)	Length (sec)
FLASH (short)	Spoiled gradient-echo	960	40	20	53
FLASH (long)	Spoiled gradient-echo	960	40	20	417
TrueFISP (short)	Steady-state free process	3.78	1.89	54	38
TrueFISP (long)	Steady-state free process	3.78	1.89	54	379
HASTE (short)	Single shot (turbo fast) spin-echo	1190	83	150	42
HASTE (long)	Single shot (turbo fast) spin-echo	1190	83	150	402

cm away from the lead tip. Configurations using two or three leads were investigated in a similar way using a second Luxtron thermometer. Before each experiment the probes were calibrated, immersed in the gel, and finally thermally equilibrated. All measurements started at the same baseline temperature.

Temperature increase was measured as the difference between the baseline temperature and the temperature reached at the end of the exposure. To reduce the measurement error, the base and maximum temperatures were averaged over 20 consecutive samples.

To calculate the local SAR from temperature measurements we followed the method described by IEEE C95.3-2002 (23). This method leads to uncertainties of about ± 1 to 2 dB in the local SAR evaluation.

Local SAR at the lead tip was calculated according to the definition of SAR by multiplying the initial slope of the temperature rise (dT/dt) by the specific heat capacity of the gel (19,21). We used a slope-determining algorithm to properly select the linear portion of the initial temperature rise. The starting point was defined as the first sharp temperature increase from baseline; the initial linear slope was estimated based on the number of samples that maximized Pearson's coefficient (R^2) of regression (range 25 to 50 samples). The slope estimation was considered reliable when Pearson's coefficient was >0.95 .

Experimental Protocols

Rectangular Box Simulator in MRI Simulator

Forty-two lead geometries were tested. The position of the PM and the lead tip was kept unchanged throughout the experiments. Different lead areas were obtained by changing the lead geometry, as explained previously. Each experiment consisted of a measurement of the baseline temperature for about 1 minute, followed by 2 minutes of RF exposure. Higher absolute temperatures would occur with prolonged exposure times.

Human-Shaped Phantom in Real MRI System

Experiments were performed on a 1.5-T scanner (Magnetom Sonata Maestro; Siemens) (Fig. 2C). The main parameters of the sequences used are summarized in Table 1. MRI parameters (TR, TE, and flip angle) were adjusted not to exceed a WB-SAR of 2 W/kg as estimated by the scanner. The torso was placed in the MRI coil and its position was adjusted to have the MRI isocenter at the lowest part of the sternum (xiphoid process), a common position in clinical practice. The lead

geometry included left and right PM placements. For each implant, three lead paths were tested (Fig. 4): without a lead loop around the PM (no-loop configuration) and with the lead forming one or two loops around the PM can (one-loop and two-loop configurations, respectively). For each lead path, the length and the position of the linear section of the lead as well as the position of the lead tip were kept constant. Only the PM was moved either to the left or to the right, without changing the sense of the winding of the loops, if any. For all experiments the total lead length was 62 cm.

The PM was interrogated before and after each scan sequence to detect any possible changes in the programmed parameters.

RESULTS

Figure 5 shows an example of temperature increase during exposure to a real MRI sequence in the human-shaped phantom and to a continuous sinusoidal RF field in the rectangular box simulator. The highest rise occurred within the first minute; a lower but stable increase was observed after 100 seconds, then an almost steady state was reached, with temperature continuing to increase, yet very slowly. After each test the PM was interrogated. No changes in any programmed parameters were observed in either the RF coil or the real MRI scanner.

Rectangular Box Simulator

The greatest temperature increase was always observed at the lead tip. No significant increase in temperature ($<1^\circ\text{C}$) was observed at the PM can or in the gel far from the lead. No differences were observed between the two PM models. The ring electrode of the bipolar leads

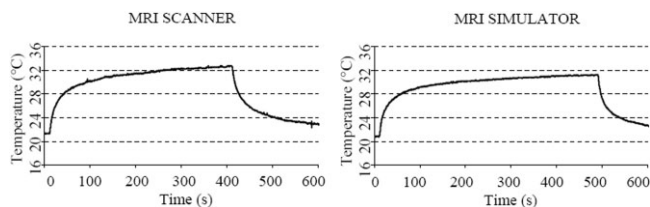


Figure 5. Example of a temperature increase during exposure to MRI RF. (Left) Temperature increase of lead tip from exposure to a clinical MRI sequence. (Right) Temperature increase during exposure to continuous sinusoidal RF from the MRI simulator.

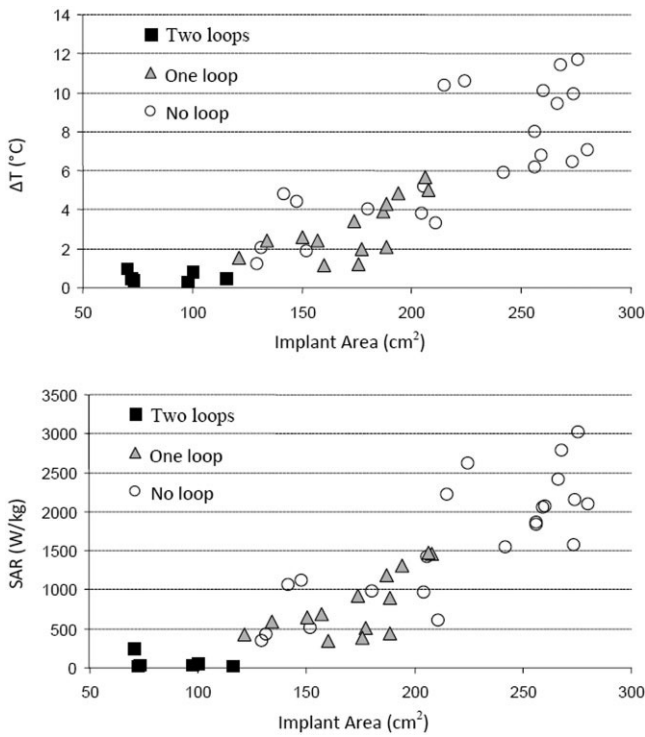


Figure 6. Plot of temperature increase (top) and local SAR at the lead tip (bottom) as a function of the lead area, from experiments performed using the rectangular box simulator. Different lead areas were obtained either by wrapping the lead around the PM can or by changing the lead path. Local SAR was estimated using the slope of the temperature increase (see text).

showed a much smaller temperature increase than the lead tip in all measurements. We observed no differences in the temperature of the lead tips whether unipolar or bipolar, or when PM programming was changed from unipolar to bipolar sensing/pacing. When the PM was connected to multiple leads simultaneously (right atrium, right and left ventricles), we did not observe a significant change in the amount of heating of each lead tip with respect to the single lead configuration.

Figure 6 (top image) shows the temperature increase at the lead tip for various lead areas; the bottom image shows the local SAR values at the lead tip, for the same experiments, plotted as a function of the lead area. As the lead area increased, we observed an increase in final temperature and the local SAR. Figure 7 shows the temperature increase at the lead tip as a function of the exposed lead length. Note that geometries with short exposed lengths always indicated negligible temperature increases, whereas, as the exposed length increased, the heating increased with lead tip heating up to 12°C. The increase of temperature and local SAR at the lead tip seems to be related to the lead area and the exposed lead length (Fig. 6). The lead around the PM can or the number of loops did not seem to play a significant role. The no-loop and one-loop configurations, with the same lead areas, produced a similar temperature increase and local SAR. However, the no-loop configuration showed, with increasing lead area,

increased heating and local SAR values. Two experiments showed a temperature increase and local SAR values significantly higher than what could be expected from their relatively large lead area. A retrospective analysis of these configurations showed that the lead had a relatively long, straight path (approximately 20 cm). Based on our experiments we cannot conclude whether a straight lead is always more heated than other lead paths.

All of the aforementioned measures were done with the center of the box positioned in the isocenter of the RF coil.

Human-Shaped Phantom

The temperature increase and local SAR values for the experiments using a real MRI scanner are reported in Table 2. As for the clinical sequences, the gradient-echo (FLASH) induced no detectable temperature increase (below the Luxtron probe sensitivity, 0.1°C) in all configurations tested. Sequences with a relatively high WB-SAR, led to temperature increases of up to 12.3°C. When the PM was implanted in the left chest area, the lead area involved in the lead path appeared to be the major factor relevant for the lead heating. The no-loop configuration (large lead area) always showed a greater temperature increase than one- and two-loop configurations.

Surprisingly, when the PM was implanted in the right chest area, the lead length seemed to play a major role; that is, the no-loop configuration again always showed temperature increases significantly greater than the one- and two-loop configurations. In addition, the temperature increases were always greater than those for the left implants. In both left and right implants the temperature increase and local SAR were proportional to the WB-SAR reported by the scanner.

The comparison between short and long sequences showed that, as observed during continuous sinusoidal

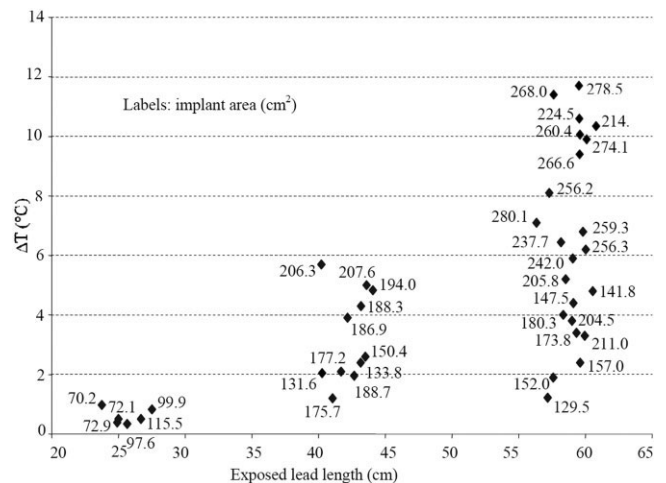


Figure 7. Plot of the temperature increase at the lead tip as a function of the exposed lead length, from the same experiments as in Figure 6. Exposed lead length was defined as the length of lead not wrapped around the PM can. The three clusters of data correspond to the no-loop, one-loop, and two-loops lead configurations, respectively.

Table 2
Temperature Increase (°C) and Lead Tip Local SAR (W/kg) of Human-Shaped Phantom Experiments*

Geometry	Left pectoral implant			Scanner reported SAR [†] (W/kg)	Right pectoral implant			Scanner reported SAR [†] (W/kg)
	No loop	One loop	Two loops		No loop	One loop	Two loops	
Exposed length (cm)	61.1	36.8	18.9		61.1	36.8	18.9	
FLASH (short)	0.1 (-)	<0.1 (-)	<0.1 (-)	0.02	<0.1 (-)	<0.1 (-)	<0.1 (-)	0.02
FLASH (long)	0.1 (-)	<0.1 (-)	<0.1 (-)	0.02	<0.1 (-)	<0.1 (-)	<0.1 (-)	0.02
TrueFISP (short)	4.2 (1055)	0.6 (-)	0.4 (-)	1.72	8.2 (2192)	1.9 (-)	0.6 (-)	1.70
TrueFISP (long)	6.2 (1255)	1.0 (-)	0.6 (-)	1.70	12.3 (2375)	2.5 (536)	1.0 (-)	1.70
HASTE (short)	6.9 (2214)	1.0 (281)	0.7 (291)	1.96	9.4 (2871)	2.1 (643)	0.7 (365)	1.94
HASTE (long)	6.3 (1362)	0.9 (-)	0.7 (-)	1.70	11.9 (2345)	2.7 (641)	1.0 (-)	1.72

-, SAR not estimable, due to low temperature increase.

*WB-SAR calculated by the MRI scanner is also reported.

[†]SAR: WB-SAR calculated by the MRI scanner.

RF exposure in the rectangular box simulator, the largest temperature increase occurred within the first minute. Figure 4 summarizes the local SAR and heating at the lead tip during a short fast spin-echo sequence for the six geometries tested.

All experiments were repeated with changing MRI parameters, such as the center of view (chest, abdomen, and pelvis) and the field of view (200, 300, and 400 mm), but also with various PM settings (unipolar vs. bipolar sensing and pacing, pacemaker on and off), without significant changes in the heating.

DISCUSSION

The major objective of this study was to determine the effect of implant geometry on the lead tip heating. Previous studies investigating MRI-induced PM lead heating reported a large variability in the induced heating. All investigations showed that the maximum RF-induced heating occurred at the lead tip. However, temperature increases at the lead tip have been reported to vary between 0.1°C (14) and 63.1°C (13).

Such variability depends on a number of factors, such as the type and positioning of the temperature probes next to the lead tip, the WB-SAR used, the cooling effect of the blood flow, the lead structure, the lead length, the geometry of the PM implant, the location of the implant in the RF coil, and the position inside the body.

Previous studies stated that the lead area, which is the area formed by the lead, the PM can, and the straight line connecting the lead tip to the PM can, plays a significant role in lead tip heating (13,19). Most of our experiments were performed to quantify the contribution of the implant area to the heating, as an independent parameter. Our data clearly show a temperature increase proportional to the lead area, although, in some cases, similar lead areas gave different temperature increases. Thus, the implant area may not be the only factor determining the temperature increase. We also found that wrapping the excess lead near the PM can does not contribute to lead tip heating; that is, given comparable implant areas, the presence of loops did not systematically affect the temperature increase produced at the lead tip.

We also investigated the contribution of exposed lead length to the amount of heating (Fig. 7). We found a negligible temperature increase in all the geometries with short exposed lead length (about 20 cm), but for longer exposed leads the temperature increase ranged from 1° to 12°C. These results suggest that the lead couples with the electric field and that large areas will also lead to RF-induced currents, because they generally imply a longer exposed lead segment. Thus, more so than area, the crucial factor that affects the amount of heating at the implant tip is the length of the exposed lead. This has also been confirmed by the high heating observed in linear lead configurations, which have been investigated in several studies (12,14,15).

We found that unipolar and bipolar leads, but also different PM settings (unipolar vs. bipolar sensing and pacing), produced similar lead heating. The lead heating obtained for a left-sided PM inside the human-shaped phantom exposed in a real MRI system was consistent with findings obtained with the rectangular box exposed in the MRI birdcage coil. The exposed lead length and the lead areas are contributing factors to lead heating. When PMs are implanted in the right side of the chest the resulting lead areas are smaller than for the left-side PMs. However, we observed a greater temperature increase, suggesting that the lead also couples to the electrical field. A resonance phenomenon in various kinds of linear structures (eg, catheters used in interventional radiology) has been hypothesized (4,15). A pacemaker lead is a conducting object embedded in an isolator, which is placed in a conducting media, thus the calculation of a resonant length has to take into account factors such as the conductivity and dielectric constant of the medium, as well as the structure of the lead (eg, number and disposition of internal conductors, insulation sheets, and the terminations at both ends). Nitz et al estimated that, at 64 MHz, the critical length ($\lambda/2$) of a conductive straight wire immersed in blood is 28.8 cm (15). This value is close to the length of the linear section of the lead in our torso simulator experiments. The induced current on the different segments of the lead may either add to, or subtract from, one another, depending on the phase of the electrical field. Such behavior may explain the differences between left and right implants. The amount of heating at

the lead tip is the result of the coupling between the local electrical field at the segments of the lead. Such coupling may result in addition- or subtraction-induced currents, depending on the phase of the local electric field.

Using a WB-SAR of approximately 1 W/kg we observed, in the worst case, a temperature rise of up to 12°C and a local SAR of up to 2300 W/kg. The *in vitro* test methods used herein were not intended to simulate the dynamics of blood and body fluids, but rather to simulate the nearly instantaneous energy deposition. Thus, for patients, the temperature rise may be reduced by blood flow.

In bipolar leads we also measured the temperature increase at the ring electrode and found very limited heating (<2°C). Similar results were found by other groups (19). The larger surface area of the ring electrode reduces the current density and therefore the temperature increase is much lower compared with the lead tip.

In our investigation of whether other PM settings could change the lead heating we found that lead heating is insensitive to PM programming (eg, unipolar/bipolar sensing and pacing) and that there were no significant differences between bipolar and unipolar leads. The simultaneous use of two or three leads did not change the heating systematically.

Baker et al (18) demonstrated that the WB-SAR calculated by different MRI systems is not a reliable metric for RF-induced heating. In addition, the methods used by the various manufacturers in calculating SAR values are not only different but in some cases proprietary, and thus it becomes rather difficult to compare results obtained with different scanners, even with the same value of WB-SAR.

We found similar differences when we compared, for a given WB-SAR, the heating obtained in the calibrated simulator with a real MRI system. Using the simulator with a calorimetrically measured WB-SAR of 1.0 W/kg we detected a temperature increase of about 12°C for a given lead configuration. In a real MRI system the same configuration showed an increase of about 6°C for a WB-SAR (as reported by the MRI system) of 1.70 W/kg. An overestimation of the WB-SAR by the real MRI system may explain the disparity. In this case, the real MRI system overestimated the WB-SAR by a factor of 3.4. Such a WB-SAR overestimation may lead to the same factor for underestimation of implant heating because most testing of implant heating relates the temperature increase to the WB-SAR given by the MRI system (M-WB-SAR). This may be due to the use of different assumptions and algorithms by the MRI systems and also to the fact that M-WB-SAR estimation might not be valid for phantoms. Further research and a comparison and re-evaluation of WB-SAR estimation and the SAR distribution of real MRI systems for humans and phantoms are urgently needed to resolve this problem.

In conclusion, our data show that the amount of MRI-induced lead tip heating strongly depends on the implant geometry, consisting of the lead area, the exposed lead length, and the position of the implant in the phantom. Critical lead tip heating was found for the longer leads. Therefore, to minimize MRI-induced lead

tip heating the PM lead should be as short as possible. Implants with a relatively large lead area (i.e., 250 to 300 cm²), exposed to a WB-SAR of about 1 W/kg, may heat at the lead tip up to 12°C with a local SAR of up to 3000 W/kg. Significant heating may also occur for smaller lead areas, depending on the degree of coupling with the electric field. An estimation of lead heating, however, is very complicated because it involves several factors aside from implant geometry, such as lead structure, lead dimension, and relative position within the MRI coil. In conclusion, implant geometry has to be accounted for as an important factor with regard to the wide variations in temperature increase reported in the literature. Future MRI-compatible pacemaker systems should aim to minimize the lead length.

Study Limitation

Our study investigated only the heating of MRI on pacing leads *in vitro*. Other potential risks of MRI in pacemaker recipients, such as fast pacing, inhibition of stimulation, or direct stimulation of the heart caused by the RF or gradient fields, require further investigation.

DISCLAIMER

The opinions and conclusions stated in this study are those of the authors and do not represent the official position of the Department of Health and Human Services. The mention of commercial products, their sources, or their use in connection with the materials reported herein is not to be construed as either an actual or implied endorsement of such products by the Department of Health and Human Services.

ACKNOWLEDGMENTS

The authors thank G. Gaggini (Sorin Biomedica Cardio) for providing the PMs and their leads; Monica Brocco for language revision of the manuscript; Giorgio De Angelis for preparation of the human-shaped phantom; Professor Paolo Pavone for suggestions on the MRI clinical sequences; Aniello Cipolletta for the assistance during MRI scanning; and Rosanna Pinto and Giorgio Lovisolo (Italian National Agency for New Technologies, Energy and the Environment) for the measurement of the electrical conductivity of the gel.

REFERENCES

1. Fetter J, Aram G, Holmes DR Jr, et al. The effects of nuclear magnetic resonance imagers on external and implantable pulse generators. *Pacing Clin Electrophysiol* 1984;7:720-727.
2. Kanal E, Borgstede JP, Barkovich AJ, et al. American College of Radiology white paper on MR safety. *AJR Am J Roentgenol* 2002; 178:1335-1347.
3. Gimbel JR, Johnson D, Levine PA, et al. Safe performance of magnetic resonance imaging on five patients with permanent cardiac pacemakers. *Pacing Clin Electrophysiol* 1996;19:913-919.
4. Duru F, Luechinger R, Scheidegger MB, et al. Pacing in magnetic resonance imaging environment: clinical and technical considerations on compatibility. *Eur Heart J* 2001;22:113-124.

5. Zaremba L. FDA guidance for MR system safety and patient exposures: current status and future considerations. In: Shellock FG, editor. *Magnetic resonance procedures: health effects and safety*. Boca Raton, FL: CRC Press; 2001. p 183–196.
6. Shellock FG. Cardiac pacemakers and implantable cardioverter defibrillators. In: *Reference manual for magnetic resonance safety, implants and devices*. Los Angeles, CA: Biomedical Research Publishing Group; 2007. p 163–176.
7. Luechinger R, Duru F, Scheidegger MB, et al. Force and torque effects of a 1.5-Tesla MRI scanner on cardiac pacemakers and ICDs. *Pacing Clin Electrophysiol* 2001;24:199–205.
8. Shellock FG, Tkach JA, Ruggieri PM, et al. Cardiac pacemakers, ICDs, and loop recorder: evaluation of translational attraction using conventional (“long-bore”) and “short-bore” 1.5- and 3.0-Tesla MR systems. *J Cardiovasc Magn Reson* 2003;5:387–397.
9. Luechinger R, Duru F, Zeijlemaker VA, et al. Pacemaker reed switch behavior in 0.5, 1.5, and 3.0 Tesla magnetic resonance imaging units: are reed switches always closed in strong magnetic fields? *Pacing Clin Electrophysiol* 2002;25:1419–1423.
10. Erlebacher JA, Cahill PT, Pannizzo F, et al. Effect of magnetic resonance imaging on DDD pacemakers. *Am J Cardiol* 1986;57:437–440.
11. Hayes DL, Holmes DR Jr, Gray JE. Effect of 1.5 Tesla nuclear magnetic resonance imaging scanner on implanted permanent pacemakers. *J Am Coll Cardiol* 1987;10:782–786.
12. Achenbach S, Moshage W, Diem B, et al. Effects of magnetic resonance imaging on cardiac pacemakers and electrodes. *Am Heart J* 1997;134:467–473.
13. Sommer T, Vahlhaus C, Lauck G, et al. MR imaging and cardiac pacemakers: in-vitro evaluation and in-vivo studies in 51 patients at 0.5 T. *Radiology* 2000;215:869–879.
14. Luechinger R, Zeijlemaker VA, Pedersen EM, et al. In vivo heating of pacemaker leads during magnetic resonance imaging. *Eur Heart J* 2005;26:376–383.
15. Nitz WR, Oppelt A, Renz W, et al. On the heating of linear conductive structure as guide wires and catheters in interventional MRI. *J Magn Reson Imaging* 2001;13:105–114.
16. Roguin A, Zviman MM, Meininger GR, et al. Modern pacemaker and implantable cardioverter/defibrillator systems can be magnetic resonance imaging safe. In vitro and in vivo assessment of safety and function at 1.5 T. *Circulation* 2004;110:475–482.
17. Rezai AR, Finelli D, Nyenhuis JA, et al. Neurostimulation systems for deep brain stimulation: in vitro evaluation of magnetic resonance imaging-related heating at 1.5 Tesla. *J Magn Reson Imaging* 2002;15:241–250.
18. Baker KB, Tkach JA, Nyenhuis JA, et al. Evaluation of specific absorption rate as a dosimeter of MRI-related implant heating. *J Magn Reson Imaging* 2004;20:315–320.
19. Ruggiera PS, Witters DM, von Maltzahn G, et al. In vitro assessment of tissue heating near metallic medical implants by exposure to pulsed radio frequency diathermy. *Phys Med Biol* 2003;48:2919–2928.
20. American Society for Testing and Material (ASTM). Designation F2182–02a. Standard test method for measurement of radio frequency induced heating near passive implants during magnetic resonance imaging. West Conshohocken, PA: ASTM; 2004.
21. Bassen H, Kainz W, Mendoza G, et al. MRI-induced heating of selected thin wire metallic implants—laboratory and computational studies—findings and new questions raised. *Minim Invasive Ther Allied Technol* 2006;15:76–84.
22. Mattei E, Triventi M, Calcagnini G, et al. Temperature and SAR measurement errors in the evaluation of metallic linear structures heating during MRI using fluoroptic probes. *Phys Med Biol* 2007;52:1633–1646.
23. Institute of Electrical and Electronics Engineers (IEEE). C95.3-2002: recommended practice for measurements and computations with respect to human exposure to radiofrequency electromagnetic fields, 100 kHz to 300 GHz; New York: IEEE; 2002.